Int J Fract (2020) 224:261–267
https://doi.org/10.1007/s10704-020-00455-1

BRIEF NOTE

Revisiting the third Sandia Fracture Challenge: a bond-associated, semi-Lagrangian peridynamic approach to modeling large deformation and ductile fracture

Masoud Behzadinasab · John T. Foster

Received: 21 November 2019 / Accepted: 15 May 2020 / Published online: 6 June 2020

Abstract Following a recent participation in Sandia Fracture Challenge 2017, in which we identified some shortcomings associated with the peridynamic theory in predicting large deformation and ductile fracture, we recently proposed a bond-associated, semi-Lagrangian, peridynamic model that addresses the noted limitations. The new theory is employed to revisit the challenge problem. Our results show that the new approach significantly improves the predictions of ductile fracture phenomenon in this challenge.

Keywords Sandia Fracture Challenge · Peridynamics · Bond-associated · Semi-Lagrangian · Additively manufactured metal · Ductile fracture · Large deformation

1 Motivation

We previously participated in the third Sandia Fracture Challenge (SFC3), outlined in Kramer et al. (2019), to explore the capabilities of the peridynamic modeling framework in predicting large deformation and ductile fracture. The challenge involved predicting the deformations and failure behavior of an additively manufactured metal with an unconventional, complicated geometry, shown in Fig. 1, under tensile loading, given a set of common engineering calibration test data for the material under consideration. As discussed in Behzadinasab and Foster (2019), there was some discrepancy between our initial, blind predictions and the actual experimental data, which was mainly attributed to the instability issues underlying the utilized peridynamic model, in two forms: (1) material instabilities inherent in the generalized, ordinary, finite deformation constitutive correspondence theory (Foster and Xu 2018), mainly under compression loading (also, under inhomogeneous deformations) (see Behzadinasab and Foster (2020a)), and (2) unreliability of a Lagrangian peridynamic framework in solving problems involving extremely large deformation and extensive damage. Addressing these issues was the main motivation behind development of a recently proposed, bond-associated, semi-Lagrangian, constitutive correspondence, peridynamic formulation (Behzadinasab 2019; Behzadinasab and Foster 2020b). In this study, the new model is employed to revisit the challenge.

In order to probe the effectiveness of the new theory in improving our prediction capabilities of large deformation and ductile fracture (in the context of SFC3), we aimed to minimize changes to our initial attempt

M. Behzadinasab (✉)· J. T. Foster
Department of Aerospace Engineering and Engineering Mechanics, The University of Texas at Austin, Austin, TX, USA
e-mail: behzadi@utexas.edu

J. T. Foster
Hildebrand Department of Petroleum and Geosystems Engineering, The University of Texas at Austin, Austin, TX, USA
e-mail: john.foster@utexas.edu

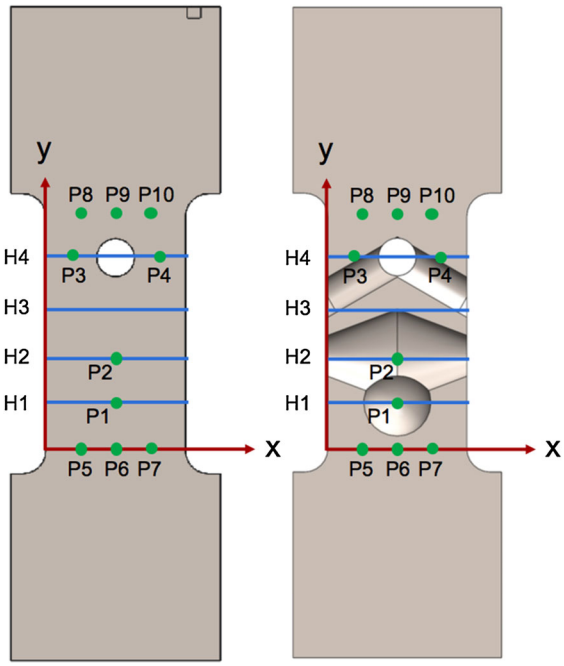

Fig. 1 Schematic of the challenge geometry (surface in left and cutaway in right) to denote the referenced locations for local strain tracking in the challenge questions (P1–P4, H1–H4) and gage displacement measurement locations (P5–P10)

in solving the challenge problem. Therefore, the same discrete systems (particle arrangements), horizon size, and calibration data are used in revisiting the problem. Also, an isotropic, homogeneous material, with no dependency on rate of deformation or temperature, is used in this modeling (similar to the initial approach).

In the remainder of this manuscript, a description of the implemented model formulation is given in Sect. 2. The results, including calibration of the model and its application to the SFC3 problem, are detailed in Sect. 3. The paper is concluded with a summary in Sect. 4.

2 Model formulation

We recently proposed (Behzadinasab and Foster 2020b) a non-local, bond-associated, velocity gradient

$$\underline{\mathbf{L}}(\mathbf{x})\langle\boldsymbol{\eta}\rangle = \frac{\bar{\mathbf{L}}(\mathbf{x}) + \bar{\mathbf{L}}(\mathbf{x}+\boldsymbol{\eta})}{2} + \left(\dot{\boldsymbol{\eta}} - \frac{\bar{\mathbf{L}}(\mathbf{x}) + \bar{\mathbf{L}}(\mathbf{x}+\boldsymbol{\eta})}{2}\cdot\boldsymbol{\eta}\right) \otimes \frac{\boldsymbol{\eta}}{|\boldsymbol{\eta}|^2},$$

in which $\underline{\mathbf{L}}(\mathbf{x})\langle\boldsymbol{\eta}\rangle$ is the velocity gradient associated with the bond $\boldsymbol{\eta} : \mathbf{x} \rightarrow \mathbf{x}+\boldsymbol{\eta}$ in the neighborhood of material point $\mathbf{x}$ in the current, deformed configuration. $\bar{\mathbf{L}}(\mathbf{x})$ is the velocity gradient at $\mathbf{x}$, which is determined through an integration of the collective deformation of the neighborhood

$$\bar{\mathbf{L}}(\mathbf{x}) = \left(\int_{\mathcal{H}(\mathbf{x})} \underline{\omega}\langle\boldsymbol{\eta}\rangle\, \dot{\boldsymbol{\eta}} \otimes \boldsymbol{\eta}\, \mathrm{d}\boldsymbol{\eta}\right) \mathbf{M}^{-1}(\mathbf{x}),$$

where $\mathbf{M}$ is called the *spatial shape tensor*, given as

$$\mathbf{M}(\mathbf{x}) = \int_{\mathcal{H}(\mathbf{x})} \underline{\omega}\langle\boldsymbol{\eta}\rangle\, \boldsymbol{\eta} \otimes \boldsymbol{\eta}\, \mathrm{d}\boldsymbol{\eta}.$$

Note that this framework is established using a semi-Lagrangian view, i.e., the peridynamic bonds and families are defined in the current, deformed domain; thus,

$$\mathcal{H}(\mathbf{x}) = \{\mathbf{x}+\boldsymbol{\eta} \mid \mathbf{x}+\boldsymbol{\eta} \in \mathcal{B}, \quad 0 < |\boldsymbol{\eta}| \leq \delta\},$$

where $\mathcal{B}$ is the peridynamic body, and δ is called the *horizon*.

This formulation results in the following force vector state:

$$\underline{t}_i(\mathbf{x})\langle\boldsymbol{\eta}\rangle = \frac{1}{2}\left[\int_{\mathcal{H}(\mathbf{x})} \left(\frac{1}{\omega_0(\mathbf{x})} + \frac{1}{\omega_0(\mathbf{x}+\boldsymbol{\xi})}\right) \underline{\omega}\langle\boldsymbol{\xi}\rangle\, \underline{\sigma}_{ij}\langle\boldsymbol{\xi}\rangle \times \left(\delta_{pj} - \frac{\xi_p \xi_j}{|\boldsymbol{\xi}|^2}\right) \mathrm{d}\boldsymbol{\xi}\right] M^{-1}_{lp}(\mathbf{x})\, \underline{\omega}\langle\boldsymbol{\eta}\rangle\, \eta_l + \frac{\underline{\omega}\langle\boldsymbol{\eta}\rangle}{\omega_0(\mathbf{x})} \underline{\sigma}_{ij}\langle\boldsymbol{\eta}\rangle \frac{\eta_j}{|\boldsymbol{\eta}|^2},$$

where $\underline{\sigma}$ is the bond-associated Cauchy stress, which is the power conjugate of the velocity gradient, and is determined using a local constitutive theory.

In this study, to maintain material objectivity, the numerical algorithm of Flanagan and Taylor (1987) is utilized to integrate the adopted constitutive equation in rate form using a co-rotational stress rate. An isotropic hardening power-law material law is used to describe the behavior of the interested material, i.e.,

$$\sigma_y = \sigma_0 \left(1 + \varepsilon_p/\varepsilon_0\right)^n,$$

where ε_p is the equivalent plastic strain, σ_0 is the initial yield stress, and ε_0 and n are constants to govern the hardening shape of yield surface.

The bond-associated internal properties, e.g. stress and strain values, can be utilized to develop a bond-

Table 1 Calibrated model parameters, extracted by the optimization procedure involving an inverse method

E (GPa)	ν	σ_0 (MPa)	ε_0	n	d_1	d_2
198	0.3	540	0.34	0.64	0.76	0.95

associated damage correspondence model, to incorporate local failure theories within the peridynamic framework. There exist many well-established fracture criteria in the classical (local) community. Some of the more complex damage theories, such as the models of Johnson and Cook (1985) and Bai and Wierzbicki (2008), involve multiple variables which would require several different experimental test data to calibrate. Using only a limited set of independent data (here 2, a longitudinal tensile test and a notched test) to tune a complicated damage model may result in a poorly calibrated model (Wierzbicki et al. 2005), which works well for the training set but poorly in other tests (similar to overfitting in statistics). Therefore, in this study we seek simpler, yet established models to simulate fracture phenomena.

Brozzo et al. (1972) proposed a damage model that takes into account the influence of hydrostatic stress on ductile failure, yet involves only a single model constant, called the *tearing parameter* TP that evolves damage over the plastic strain as

$$TP = \int \frac{2\sigma_T}{3(\sigma_T - \sigma_m)} \, \mathrm{d}\varepsilon_p,$$

where σ_T is the maximum principal stress, and σ_m is the hydrostatic stress. In this model, the material fails once its tearing parameter reaches a critical value. Wellman (2012) investigated Brozzo's theory and showed that while it captures damage in simpler problems, it is not well-suited to more complex scenarios (statistically speaking, the model has a high bias). They modified the original formulation in two ways: (1) introduction of a Heaviside function on the maximum principal stress, to limit damage growth to tensile loading, and (2) including a power-law form to the stress-state portion of the equation, i.e.,

$$TP = \int \left\langle \frac{2\sigma_T}{3(\sigma_T - \sigma_m)} \right\rangle^4 \mathrm{d}\varepsilon_p,$$

in which the fourth power was chosen by considering some tested materials. Inspired by these works, we include the following damage model in this study:

$$\dot{\underline{D}} = \begin{cases} d_1 \left\langle \dfrac{2\underline{\sigma}_T}{3(\underline{\sigma}_T - \underline{\sigma}_m)} \right\rangle^{d_2} \dot{\underline{\varepsilon}}_p & \text{if } \underline{D} < 1, \\ 0 & \text{otherwise,} \end{cases}$$

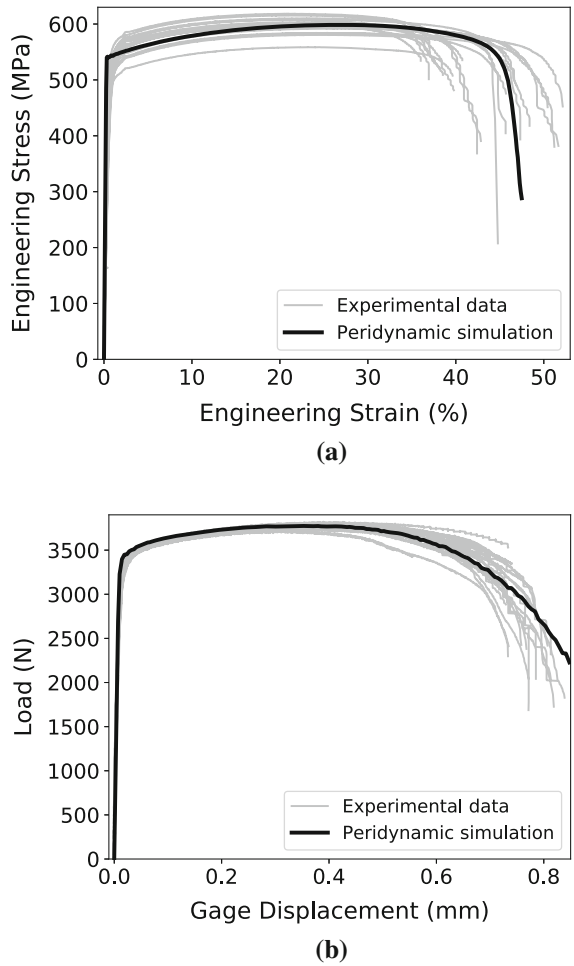

Fig. 2 Comparison of the macroscopic behavior of the material between the simulations (new model) and experiments for the longitudinal tensile test (**a**) and notched calibration test (**b**). Gray color indicates the experimental data, and black shows the model results

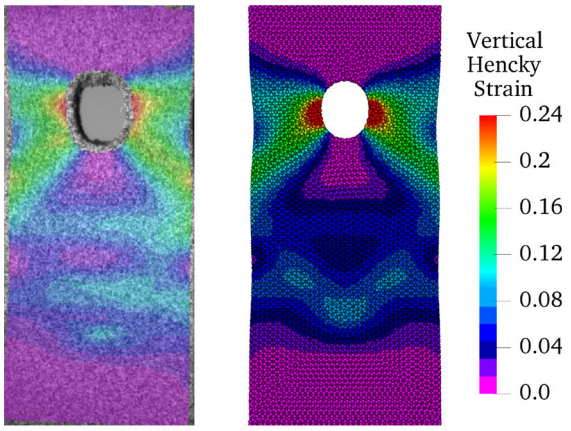

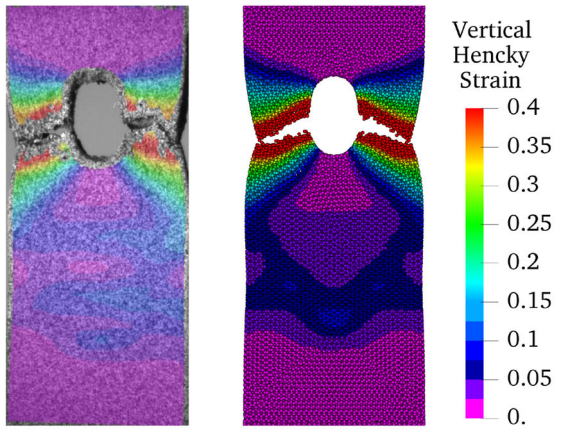

Fig. 3 Contours of vertical Hencky strains compared between the experimental DIC measurements (EXP) and peridynamic simulations (SIM) at crack initiation (CI) (**a**, **b**) and complete failure (CF) (**c**, **d**)

where $\underline{D}, \underline{\sigma}_T, \underline{\sigma}_m$, and $\underline{\varepsilon}_p$ are the bond-associated damage, maximum principal stress, hydrostatic stress, and equivalent plastic strain, respectively. d_1 and d_2 are model constants here. A possible way to model failure is to break a bond once its damage reaches 1 (note that d_1 is correlated to the critical tearing parameter in the original Brozzo's formula; therefore, we choose 1 to be the damage threshold limit). However, a sudden bond breakage may lead to instability issues. To avoid that, a gradual degradation of a bond strength is incorporated using the following modification of the influence state:

$$\underline{\omega}\langle\boldsymbol{\eta}\rangle = \omega_\eta(|\boldsymbol{\eta}|)\,\omega_D\big(\underline{D}\langle\boldsymbol{\eta}\rangle\big)\,,$$

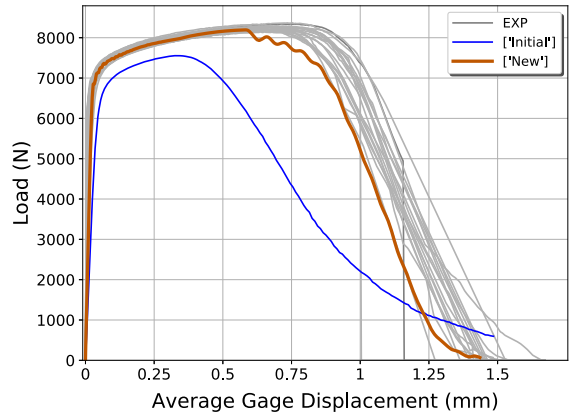

Fig. 4 Macroscopic behavior of the challenge specimen compared between the initial and new simulations, and the experiments (EXP). Evidently, the new approach has significantly improved the predictions

where $\omega_\eta(|\boldsymbol{\eta}|)$ is the conventional, spherical influence function for undamaged material. Following the remark on the role of influence function in Behzadinasab and Foster (2020b), Remark 5, ω_η is adopted as

$$\omega_\eta(|\boldsymbol{\eta}|) = \begin{cases} \dfrac{1}{|\boldsymbol{\eta}|^2}\left[1-\left(\dfrac{|\boldsymbol{\eta}|}{\delta}\right)^2\right] & \text{if } 0<|\boldsymbol{\eta}|<\delta, \\ 0 & \text{otherwise.} \end{cases}$$

ω_D is the damage-related part of the influence function that is defined as

$$\omega_D\big(\underline{D}\langle\boldsymbol{\eta}\rangle\big) = \begin{cases} \dfrac{1-\underline{D}\langle\boldsymbol{\eta}\rangle}{1-D_c} & \text{if } \underline{D}\langle\boldsymbol{\eta}\rangle > D_c, \\ 1 & \text{otherwise,} \end{cases}$$

resulting in a linear degradation of the influence function with damage. D_c is chosen to be 0.9 in this study.

3 Results

The aforementioned model is implemented in Peridigm (Parks et al. 2012), an open-source, massively parallel peridynamic code. The same modeling techniques as in our initial attempt, detailed in Behzadinasab and Foster (2019), are used here, including: (1) calibration data set—a set of longitudinal tensile and notched tensile tests, (2) discretization scheme, (3) numerical method, (4) boundary condition modeling, and (5) model calibration. Since the main motivation of this revisit is

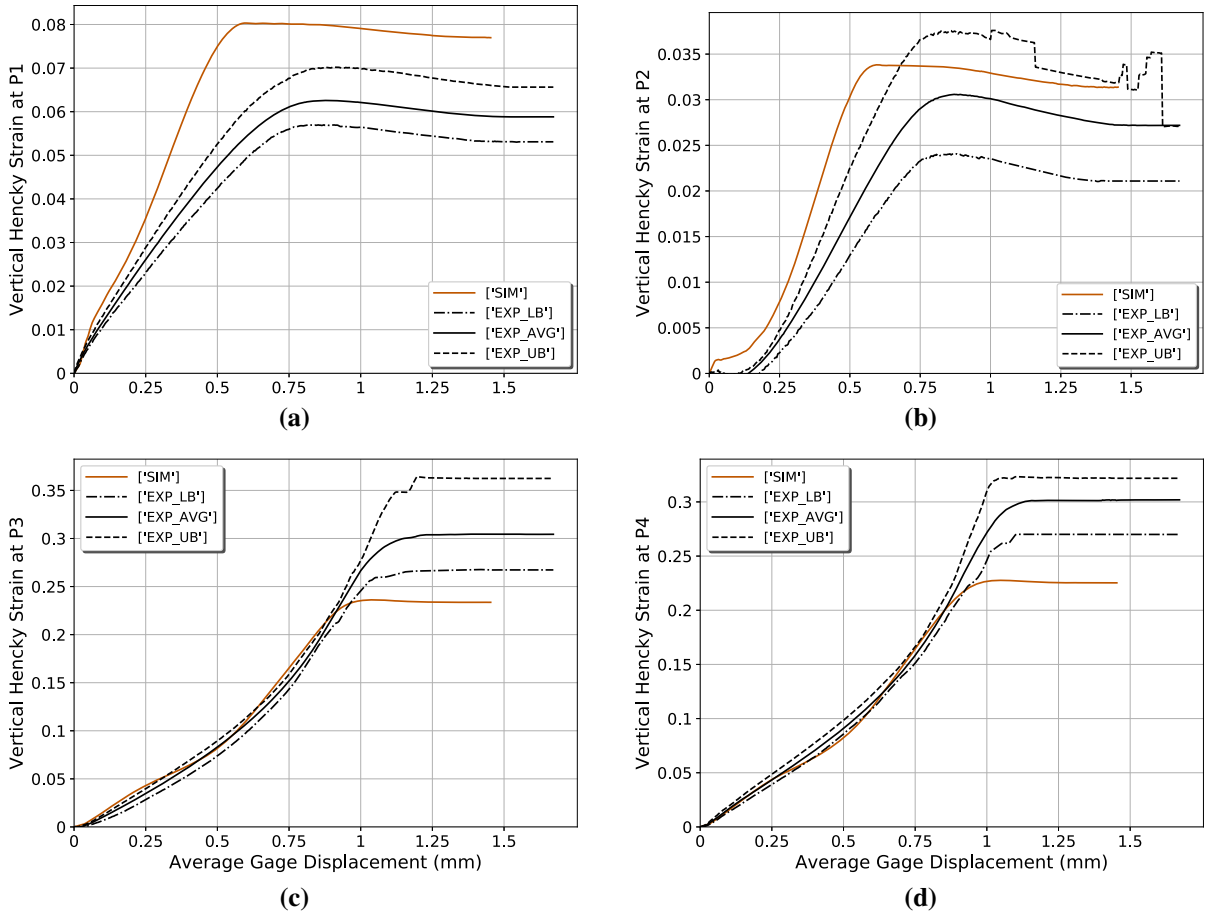

Fig. 5 Histories of the vertical logarithmic strains at P1 (**a**), P2 (**b**), P3 (**c**), and P4 (**d**) over the course of loading. The peridynamic simulations (SIM) are compared with the experimental values (EXP). Simulations refer to the new model

to evaluate the performance of the new model, we do not perform any statistical analysis here and present only the nominal response of material (in contrast to the previous modeling). All the simulations were performed on Texas Advanced Computing Center (TACC) Stampede2 clusters. 2040 processors were employed to complete the challenge simulation in 12 h.

Seven material and failure constants are involved in the calibration, using the inverse method detailed in Behzadinasab and Foster (2019), Section 3: two elasticity moduli (the Young's modulus E and the Poisson's ratio ν), three hardening parameters (σ_0, ε_0, n), and two failure variables (d_1, d_2). The calibrated parameters are provided in Table 1, and the resulting load–displacement curves are plotted in Fig. 2, showing a good agreement between the peridynamic simulations and the experiments.

We want to emphasize that experimental data from the challenge main objective is masked during the model calibration, to achieve a blind-prediction setting. The calibrated model is applied to simulate the challenge problem, *without additional changes to the calibrated parameters*. The crack path is correctly obtained from the simulation, as shown in Fig. 3. Failure initiates near the intersection between the through hole and the angled channels, then two near-symmetric cracks propagate along the channels. The failure path was also predicted accurately in our initial attempt.

Figure 4 compares the macroscopic load-displacement response of the challenge structure between the initial and new simulations, and the actual experiments. While the initial approach resulted in an underestimation of the load-carrying capacity of the structure (in both elastic and plastic regimes) and simulated an early fracture,

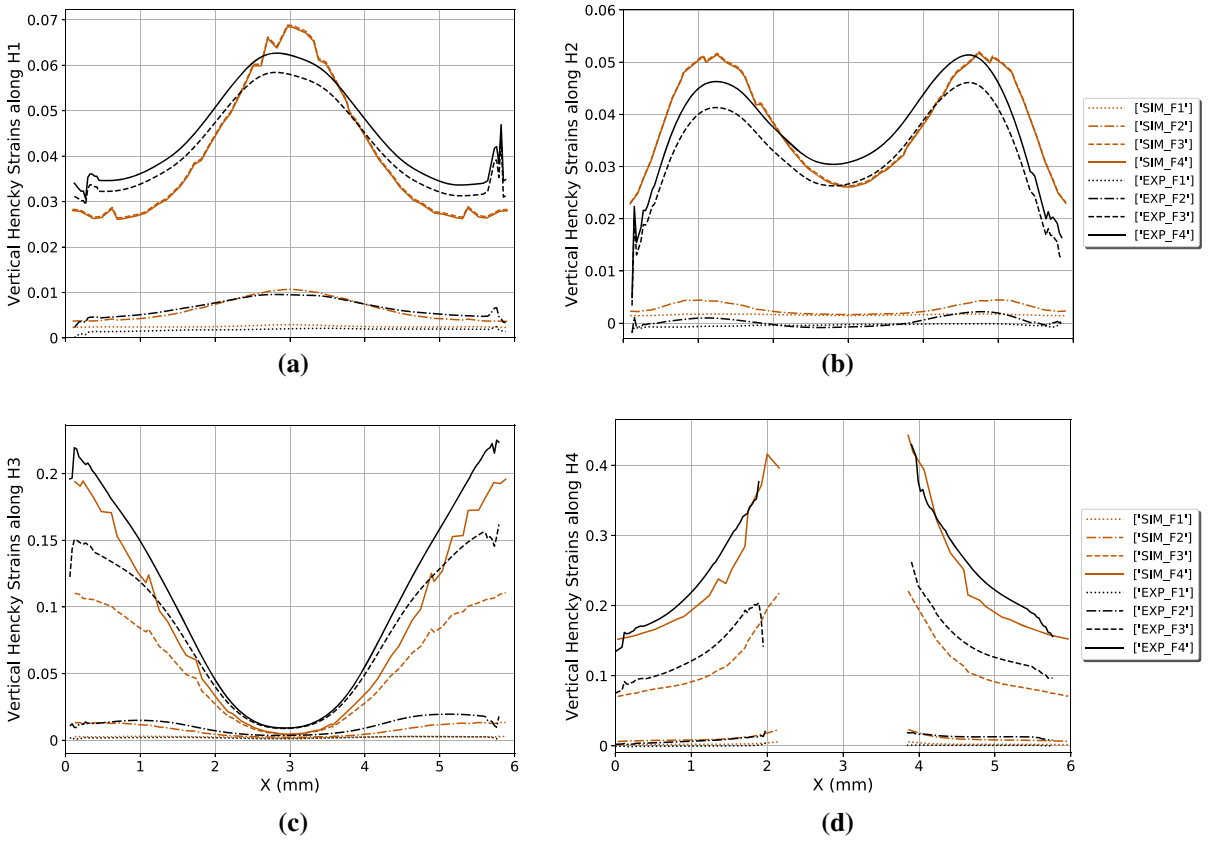

Fig. 6 Vertical logarithmic strains along four lines H1 (**a**), H2 (**b**), H3 (**c**), and H4 (**c**) at four instances of loading F1, F2, F3, and F4. The peridynamic simulations (SIM) are compared with the experimental values (EXP). Simulations refer to the new model

the new model has significantly improved the predictions. Also, note that the crack propagation speed is in agreement between the new simulations and the experiments, while the initial predictions resulted in a slow decay of the load-carrying capacity after crack initiation.

Next, the microscopic behavior of the material is compared between the simulation and experiments. Focus is on the strain measures of the surface of the challenge geometry, in which it was possible to draw experimental values using DIC measurements. Figure 3 shows the contours of vertical Hencky (logarithmic) strain values at crack initiation and complete failure. The vertical logarithmic strains at the points P1–P4 (potential sites for damage initiation, which are shown in Fig. 1) against the history of loading are shown in Fig. 5. Also, the strain values along the lines H1–H4 at four instances of loading F1 (75% of peak load, before peak), F2 (90% of peak load, before peak), F3 (peak load), F4 (90% of peak load, after peak) are compared between the experiments and simulations in Fig. 6. While the microscopic predictions are certainly not perfect, a significant improvement over the initial simulations is noted (cf. Behzadinasab and Foster 2019, Section 4). Note that here we do not attempt to interpret the physical results, as a comprehensive discussion is readily provided in the lead article of SFC3 (Kramer et al. 2019). Following the lead article results, while temperature effects appears negligible in this challenge, inclusion of anisotropy, loading rate dependencies, and geometrical imperfections can potentially improve the strain predictions.

4 Concluding remarks

The Sandia Fracture Challenge 2017 is revisited using a recently proposed, bond-associated, semi-Lagrangian, peridynamic model. It is shown that the new approach

significantly improves the predictions in the challenge, compared with the initial predictions. Based on this conclusion, we believe that the new model is capable of enhancing simulations in problems involving large deformation and ductile fracture. The improvements are mostly attributed to an enhanced model stability, by utilizing a bond-associated, rate-based peridynamic formulation.

Acknowledgements The authors are grateful for the financial support provided by the AFOSR MURI Center for Materials Failure Prediction through Peridynamics: Project NO. ONRBAA12-020. M. Behzadinasab also acknowledges the fellowship funding by The University of Texas at Austin.

References

Bai Y, Wierzbicki T (2008) A new model of metal plasticity and fracture with pressure and lode dependence. Int J Plast 24(6):1071–1096

Behzadinasab M (2019) Peridynamic modeling of large deformation and ductile fracture. PhD thesis, The University of Texas at Austin

Behzadinasab M, Foster JT (2019) The third Sandia fracture challenge: peridynamic blind prediction of ductile fracture characterization in additively manufactured metal. Int J Fract 218:97–109

Behzadinasab M, Foster JT (2020a) On the stability of the generalized, finite deformation correspondence model of peridynamics. Int J Solids Struct 182:64–76

Behzadinasab M, Foster JT (2020b) A semi-Lagrangian, constitutive correspondence framework for peridynamics. J Mech Phys Solids 137:103862

Brozzo P, Deluca B, Rendina R (1972) A new method for the prediction of formability limits in metal sheets. In: Proc 7th Biennal Conf IDDR

Flanagan D, Taylor L (1987) An accurate numerical algorithm for stress integration with finite rotations. Comput Methods Appl Mech Eng 62(3):305–320

Foster JT, Xu X (2018) A generalized, ordinary, finite deformation constitutive correspondence model for peridynamics. Int J Solids Struct 141:245–253

Johnson GR, Cook WH (1985) Fracture characteristics of three metals subjected to various strains, strain rates, temperatures and pressures. Eng Fract Mech 21(1):31–48

Kramer SL, Boyce BL, Jones A et al (2019) The third Sandia fracture challenge: predictions of ductile fracture in additively manufactured metal. Int J Fract 218:5–61

Parks ML, Littlewood DJ, Mitchell JA, Silling SA (2012) Peridigm users' guide v1. 0.0. Sandia report 7800

Wellman GW (2012) A simple approach to modeling ductile failure. Sandia National Laboratories, Albuquerque, NM, Report No SAND2012-1343

Wierzbicki T, Bao Y, Lee YW, Bai Y (2005) Calibration and evaluation of seven fracture models. Int J Mech Sci 47(4–5):719–743